Tuning the particle size, physical properties, and photocatalytic activity of Ag_3PO_4 materials by changing the Ag^+/PO_4^{3-} ratio

Hung N M[1,3], Oanh L T M[1,2,†], Chung D P[2], Thang D V[1,3], Mai V T[1,4], Hang L T[1,5], and Minh N V[1,2]

[1] *Center for Nano Science and Technology, Hanoi National University of Education, 136 Xuan Thuy Road, Cau Giay District, Hanoi 100000, Vietnam*
[2] *Department of Physics, Hanoi National University of Education, 136 Xuan Thuy Road, Cau Giay District, Hanoi 100000, Vietnam*
[3] *Hanoi University of Mining and Geology, Duc Thang Ward, North Tu Liem District, Hanoi 100000, Vietnam*
[4] *Institute of Materials Science, Vietnam Academy of Science and Technology, 18 Hoang Quoc Viet, Hanoi 100000, Vietnam*
[5] *Faculty of Basic Sciences, Hanoi University of Natural Resources and Environment, 41A Phu Dien Road, North Tu Liem, Hanoi 100000, Vietnam*

(Received 21 March 2022; revised manuscript received 27 May 2022; accepted manuscript online 28 July 2022)

This study demonstrates the influence of the Ag^+/PO_4^{3-} ratio in precursor solution on the crystal structural formation, morphology, physical properties, and photocatalytic performance of a Ag_3PO_4 photocatalyst that is fabricated, using a facile precipitation method, from $AgNO_3$ and $Na_2HPO_4 \cdot 12H_2O$. The material characterizations were carried out using x-ray diffraction (XRD), scanning electron microscopy (SEM), energy-dispersive x-ray spectroscopy (EDX), Brunauer–Emmett–Teller (BET) surface area, Fourier transform infrared (FTIR) absorption, Raman scattering, x-ray photoelectron spectroscopy (XPS), UV-vis absorption, and photoluminescence (PL). The results show that Ag_3PO_4 crystallizes better when the excess PO_4^{3-} content increases, and the lattice parameters decrease slightly, while the crystal diameter and the particle size increase. This change is also observed in the Raman scattering and FTIR spectra with the increase in the vibration frequency of the $[PO_4]$ group. The compression of the $[PO_4]$ unit was also confirmed in the XPS spectra with the shift of P 2p peaks toward higher binding energy. The photocatalytic results showed that the samples synthesized from excess PO_4^{3-} solution exhibited higher photocatalytic performance compared to the sample with a Ag^+/PO_4^{3-} ratio of 3:1. A sample prepared from the precursor solution with a Ag^+/PO_4^{3-} ratio of 3:1.5 was optimal for RhB decomposition under both visible light and natural sunlight, completely decomposing 10 ppm RhB after 15 minutes of xenon lamp irradiation and after 60 minutes under solar light irradiation. This is attributed to the high crystallinity, small particle size and low electron–hole recombination rate of the sample.

Keywords: morphology, photocatalytic, Ag^+/PO_4^{3-} ratio, visible light

PACS: 81.05.Zx, 81.07.–b, 81.16.Be **DOI:** 10.1088/1674-1056/ac84ce

1. Introduction

Recently, among various photocatalysts, silver orthophosphate Ag_3PO_4 (APO) has emerged as a breakthrough in the field of visible light photocatalysis due to its small optical band gap of 2.43 eV, high quantum efficiency, and superior photooxidative capability.[1,2] As the formation of electron/hole pairs on the surface of APO particles plays an important role in the photocatalytic performance, many studies have been carried out with the aim to control the particle size or particle morphology to increase the specific surface area.[3–6] The studies showed that synthesis parameters such as the precipitating agents,[7,8] the ratios of the starting materials,[9,10] the concentration of the reaction catalysts,[5,11] the fabrication time,[3,4,12] and pH conditions[13] greatly influence the size and morphology of the particles.

Although it possesses great potential in the field of environmental remediation and renewable energy, APO has its own disadvantages in that it consumes a large amount of silver metal due to its wide use, leading to an increase in photocatalyst costs.[4] More importantly, during photocatalytic activity, the Ag^+ ions in the APO lattice are susceptible to metallization upon receiving electrons, leading to undesirable and uncontrolled photocorrosion.[14,15] As a result, the structure of the material is destroyed over time and the photocatalytic activity decreases. This has remained a challenge for researchers so far. Therefore, besides finding solutions to increase specific surface area, researchers also focus on enhancing the structural stability of the materials by adjusting the ratio of Ag^+ and PO_4^{3-} [9,16,17] to find the most stable structure. In addition, increasing the lifetime of the electron/hole pair to increase the photocatalytic efficiency has always been of interest to research through the creation of a heterojunction between APO and other semiconductors[15,18–21] as well as doping of APO with suitable ions.[22–24]

Previous studies showed that the different concentrations of Ag^+ and PO_4^{3-} in the starting solutions significantly affects the particle size and morphology, crystallinity, absorption capability and structure stability of Ag_3PO_3. Febiyanto used the precursors of $AgNO_3$ and $Na_2HPO_4 \cdot 12H_2O$ with a given molar ratio of 3:1 and varied the concentration of both the $AgNO_3$ and Na_2HPO_4 precursor solutions. The results showed that Ag_3PO_3 prepared from the 1.0 M $AgNO_3$

†Corresponding author. E-mail: lemaioanh@gmail.com

© 2023 Chinese Physical Society and IOP Publishing Ltd

and 0.33 M $Na_2HPO_4 \cdot 12H_2O_4$ solutions exhibited the highest photocatalytic activity.[9] The authors believed that the reason for this was due to the different concentrations in the reaction solution affecting the nucleation and crystal growth during the sample preparation. Again using $AgNO_3$ and Na_2HPO_4, with no change in mass and molar ratio in different samples but with varying concentrations of ammonia added, Febiyanto[17] found that a concentration of 0.05 M ammonia was suitable for the synthesis of Ag_3PO_4 with the highest photocatalytic activity; this was increased 4.13 times compared to Ag_3PO_4 prepared without ammonia. This result was explained by the fact that the appropriate presence of ammonia successfully reduced the particle size and increased the homogeneity of the catalyst, in favor of the photocatalytic activity. Qin,[16] when using $AgNO_3$ and $NH_4H_2PO_4$ as starting materials, found that the rich Ag^+ ion Ag_3PO_4 can form the surface plasmon resonance (SPR) of Ag nanoparticles to reduce the corrosion of Ag_3PO_4, thus enhancing the photocatalytic activity and stability (highest for the sample with a Ag^+/PO_4^{3-} ratio of 3:1). Afifah[10] used $AgNO_3$ and KH_2PO_4 as reactants and changed the Ag^+/PO_4^{3+} ratio by changing the KH_2PO_4 concentration in aqueous solutions of 0.10 M, 0.15 M, 0.30 M, 0.45 M, and 0.60 M while keeping the same concentration and amount of $AgNO_3$ solution. The results show that the Ag_3PO_4 fabricated from 20 ml of 0.15 M KH_2PO_4 and 50 ml of 0.1 M $AgNO_3$ (Ag^+/PO_4^{3-} ratio of 3:1.8) exhibits superior photocatalytic activity. This is attributed to the small size of the mixture morphology of spheres and tetrahedra, high crystallinity and formation of defect sites.

Although the use of $Na_2HPO_4 \cdot 12H_2O$ as a precursor has been studied, unfortunately, the effect of the Ag^+/PO_4^{3-} ratio on the photocatalytic performance of the material has not been reported. The objective of this study was to use excess $Na_2HPO_4 \cdot 12H_2O$ as a source of phosphate ions with the hope that the excess of PO_4^{3-} would limit the aggregation of Ag^+ and thus prevent metallization to Ag^o. As a result, APO nuclei would form more easily and crystallize better. The ratio of Ag^+/PO_4^{3-} was adjusted to 3:1, 3:1.5, 3:2, and 3:3. The study focused on the investigation of the variation of crystallinity, crystal structure and other physical properties, and photocatalytic activity as a consequence of increasing excess PO_4^{3-} concentrations. In addition, to demonstrate the superior applicability of the fabricated APO, besides using visible light, photocatalytic activity was carried out under the irradiation of natural sunlight at noon.

2. Materials and methods

2.1. Materials

The chemicals used in this work are silver nitrate ($AgNO_3$, Sigma-Aldrich, 99%) and disodium hydrogen phosphate 12-hydrate ($Na_2HPO_4 \cdot 12H_2O$, Sigma-Aldrich, 99%). Rhodamine B (RhB, $C_{28}H_{31}ClN_2O_3$, Sigma-Aldrich, 95%) was used as an organic colorant in the photocatalytic test. These starting materials were used without further purification. A xenon lamp (300 W/220 V) was used as the visible light source irradiation.

2.2. Synthesis of photocatalysts

Ag_3PO_4 materials were synthesized using a facile precipitation method. Firstly, 0.5096 g of $AgNO_3$ was dissolved in 150 ml of distilled water to achieve 0.02 M Ag^+ solution (solution A). In four separate beakers, 0.1420 g, 0.2129 g, 0.2839 g, and 0.4259 g $Na_2HPO_4 \cdot 12H_2O$ were dissolved in 50 ml, 75 ml, 100 ml, and 150 ml of distilled water, respectively, to obtain the 0.02 M PO_4^{3-} solution (solution B). With these amounts of starting materials, the adjusted Ag^+/PO_4^{3-} ratio was adjusted to be 3:1, 3:1.5, 3:2, and 3:3. Next, solution A was slowly dripped into solution B to obtain a mixture of solution C. Solution C was magnetically stirred for 3 h at room temperature, and a yellow precipitate was obtained. The precipitate was filtered and washed 5 times with distilled water, and was then dried at 100 °C to obtain yellow powder Ag_3PO_4.

For convenience, the different samples are named as Ag/P 3:1, Ag/P 3:1.5, Ag/P 3:2, and Ag/P 3:3 corresponding to Ag^+/PO_4^{3-} ratios of 3:1, 3:1.5, 3:2, and 3:3, respectively.

2.3. Characterization

The crystal structure of the samples was investigated using an x-ray diffractometer (XRD, Brucker D8 Advance) with Cu $K\alpha$ ($\lambda = 1.54064$ Å) radiation over Bragg angles ranging from 20° to 90°. A scanning electron microscope (SEM, JED-2300) equipped with energy dispersive x-ray spectroscopy (EDS) was used to study the morphology and elemental composition of the samples. The Brunauer–Emmett–Teller (BET) surface area was measured by a high-performance adsorption analyzer (Micromeritics 3Flex). An FTIR/NIR spectrometer (Shimadzu IR Prestige-21) was used to carry out Fourier transform infrared spectroscopy (FTIR) of as-synthesized samples. Raman scattering spectroscopy was conducted using a Raman microscope (Horiba LabRam HR Evolution) using a 532 nm laser beam as an excitation source. UV-vis diffuse reflectance spectroscopy (DRS) was performed on a UV-vis spectrophotometer (Jasco V670). Furthermore, the surface element composition analysis of Ag_3PO_4 samples was studied using x-ray photoelectron spectroscopy with the energy resolution of 0.1 eV (XPS, Thermo Scientific Multilab-2000) using an Al $K\alpha$ monochromatized source. Photoluminescence (PL) spectroscopy was performed using a fluorescence spectrophotometer (Nanolog Horiba iHR 550) using an excitation wavelength of 350 nm.

2.4. Photocatalytic activity test

In this study, 10 ppm RhB solution was used as a color indicator to evaluate the visible-light-driven photocatalytic performance of APO in the decomposition of organic molecules. A xenon lamp (300 W/220 V) was used as the excitation visible light source. At the same time, natural sunlight was also used as a reference measurement.

Firstly, 0.06 g of APO was dissolved in 30 ml of distilled water and then magnetically stirred for 30 min. Secondly, 30 ml of 20 ppm RhB solution was added to the above solution (the final concentration of RhB solution for photocatalysis was 10 ppm). The mixture was magnetically stirred in a dark chamber for 30 min to reach an adsorption–desorption equilibrium state. After dark stirring, the solution was illuminated under a xenon lamp using a UV cut-off filter to investigate the visible-light-driven photocatalytic properties of the sample. The distance between the xenon lamp and the surface of the RhB solution is 10 cm (illuminance of 23121 lux). After each 5 minutes (or 10 minutes), 4 ml of RhB solution was removed and centrifuged at 4000 rpm to remove the APO powder. The concentration of RhB remaining in the solution at a time was assessed via the absorption spectrum of the solution. The absorption intensity of the characteristic absorption peak of RhB at 554 nm was used to determine the remaining content of RhB in the solution at a time using a standard curve that represents the relationship between RhB concentration and absorbance.

To evaluate the practical applicability of APO, natural sunlight at noon (illuminance of 32766 lux) was used as an excitation source for the photocatalysis of the material. The steps were similar to those of the above photocatalytic process using xenon light.

3. Results and discussion

The crystal structures of the as-synthesized samples were determined using x-ray diffraction (XRD) measurements. Figure 1(a) shows XRD patterns of the products with different Ag^+/PO_4^{3-} ratios (3:1; 3:1.5; 3:2; 3:3) in precursor solutions. All the patterns match well with JCPDS card No. 06-0505 with no strange peak, indicating that the samples are pure Ag_3PO_4 with a body-centered cubic structure and space group $P4\text{-}3n$. The sharp peaks with small full-width half maxima (FWHM) of the peaks reveal that the samples were well crystallized. Using the positions and FWHM of the reflection planes, the lattice parameters and the crystal diameter were calculated. The results show $a = b = c \sim 5.989$ Å and $D_{XRD} \sim 44$ nm for the Ag/P 3:1 sample, which are relatively consistent with previous studies.[4,9,12] Figure 1(b) depicts a comparison of the position of the sharp peak (210) between different samples, which shows a shift towards a larger 2θ angle as the Ag^+/PO_4^{3-} ratio decreases. This leads to a slight decrease in lattice parameters, as shown in Table 1. In contrast to the decrease in lattice parameters, the crystal size increased, which showed an increase in crystallinity as the PO_4^{3-} content increases. This may be due to the high concentration of PO_4^{3-} that inhibits the metallization of Ag^+ ions and stimulates the formation of crystal nuclei, which helps APO crystals grow stronger.

Table 1. Lattice parameters, crystallite and nanoparticle diameters, and specific surface areas of the as-synthesized Ag_3PO_4 with different Ag^+/PO_4^{3-} ratios in precursor solution (Ag^+/PO_4^{3-} = 3:1, 3:1.5; 3:2; 3:3).

Samples	Lattice parameters $a = b = c$ (Å)	Diameter of crystallite D_{XRD} (nm)	Particle diameter D_{SEM} (nm)	Specific surface area (m^2/g)
Ag/P 3:1	5.989	44	~ 160	2.8
Ag/P 3:1.5	5.968	48	~ 175	3.0
Ag/P 3:2	5.972	41	~ 215	1.8
Ag/P 3:3	5.968	49	~ 230	1.8

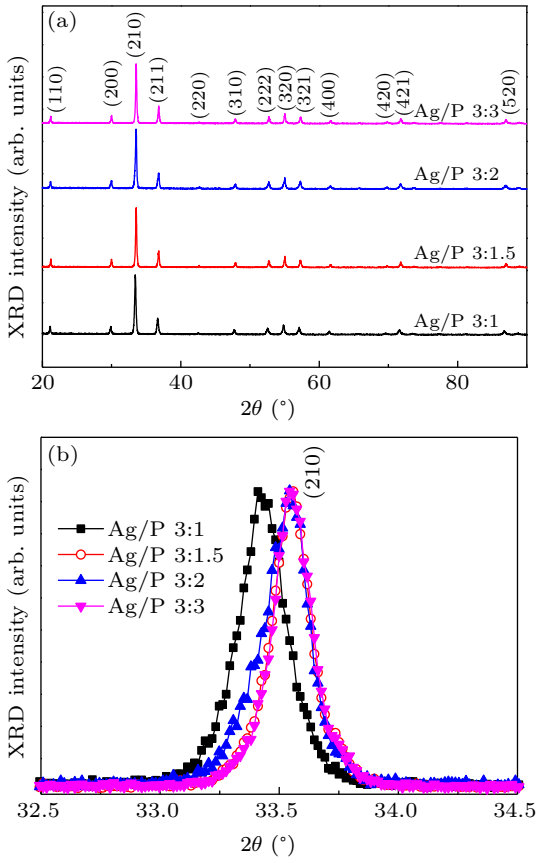


Fig. 1. (a) XRD patterns of the as-synthesized Ag_3PO_4 with different Ag^+/PO_4^{3-} ratios in precursor solution (Ag^+/PO_4^{3-} = 3:1; 3:1.5; 3:2; 3:3) and (b) a comparison of the (210) peak position.

Figure 2 shows the scanning electron microscope (SEM) images of the as-synthesized Ag_3PO_4 samples. All the samples possess a spherical morphology with relatively uniform particle size. It is obvious that the size of particles increases with increasing PO_4^{3-} content. The particle size distribution, determined using ImageJ software, showed that the average grain sizes of the samples were approximately 160 nm,

175 nm, 215 nm, and 230 nm for samples Ag/P 3:1, Ag/P 3:1.5, Ag/P 3:2, and Ag/P 3:3, respectively. This suggests that the excess PO_4^{3-} concentration not only stimulates crystal growth, but also promotes agglomeration of crystals to produce larger particles. It is a fact that if the concentration of PO_4^{3-} is low, the Ag^+ ions with a small radius meet each other with a higher probability, promoting metallization to Ag^o. Therefore, increasing the concentration of PO_4^{3-} will limit the metallization of Ag^+ and increase the probability of APO crystal nucleation, leading to faster growth of APO crystals, resulting in larger grain sizes.

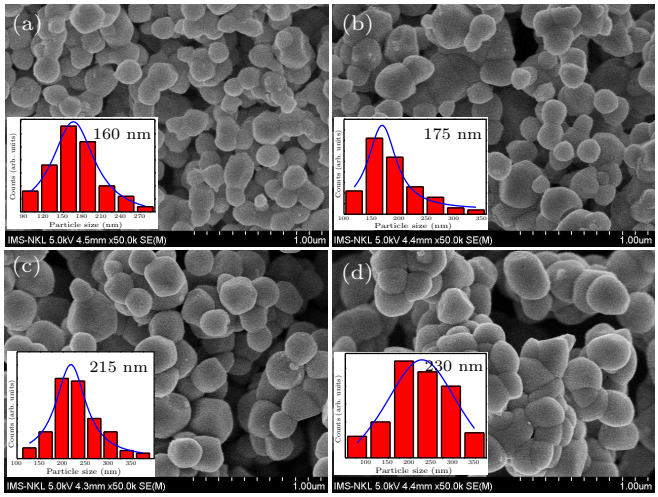


Fig. 2. SEM images of as-synthesized Ag_3PO_4 with different Ag^+/PO_4^{3-} ratios in precursor solution of (a) 3:1, (b) 3:1.5, (c) 3:2, and (d) 3:3.

Energy-dispersive x-ray spectroscopy (EDX) was used to analyze the elemental composition of the as-synthesized samples. Figure 3(a) shows that all the peaks are consistent with the component elements of the Ag_3PO_4 crystal: Ag, O, and P. The results of the BET specific surface analysis, performed via nitrogen adsorption–desorption measurements, are presented in Fig. 3(b) and Table 1. Table 1 shows that the specific surface area of the as-synthesized samples is quite small, only about 2 m^2/g–3 m^2/g, relatively consistent with previous reports.[12,25,26] Therefore, although figure 3(b) shows the separation of the adsorption and desorption curves, the difference in absolute quantitative adsorbed values between them is not significant. It is well known that the large surface area provides a more active center for photocatalytic activity, thereby increasing the photocatalytic efficiency. However, with this result, it can be predicted that the adsorption capacity of the as-prepared sample is small; the photocatalytic efficiency is not caused by the large surface area, but mainly relies on the photocatalytic activity of the material itself.

Figure 4(a) presents the FTIR spectra of the prepared APO samples. It is clear that all the required characteristic absorption bands of APO were depicted. The signals at 1635 cm^{-1} and 3435 cm^{-1} were attributed to the bending and stretching modes of adsorbed water molecules. The absorption peaks at 2350 cm^{-1} can be assigned to the asymmetric stretching mode (ν_3) of absorbed CO_2 on the surface of APO.[27] The characteristic bands of PO_4 groups appeared at 560 cm^{-1} (antisymmetric bending mode ν_4) and 1015 cm^{-1} (antisymmetric stretching ν_3).[28,29] In addition, the band at 1390 cm^{-1} can be assigned to nitrate groups resulting from synthesis residuals. It can be deduced that the FTIR spectra have indirectly reflected the presence of components constituting the synthesized sample. A detailed comparison of the FTIR peak position at 1015 cm^{-1} is presented in Fig. 4(b). A small shift of the vibrational frequency towards higher wave numbers was observed as the PO_4^{3-} concentration increased, which is consistent with the slight decrease in the lattice constant observed in the XRD results.

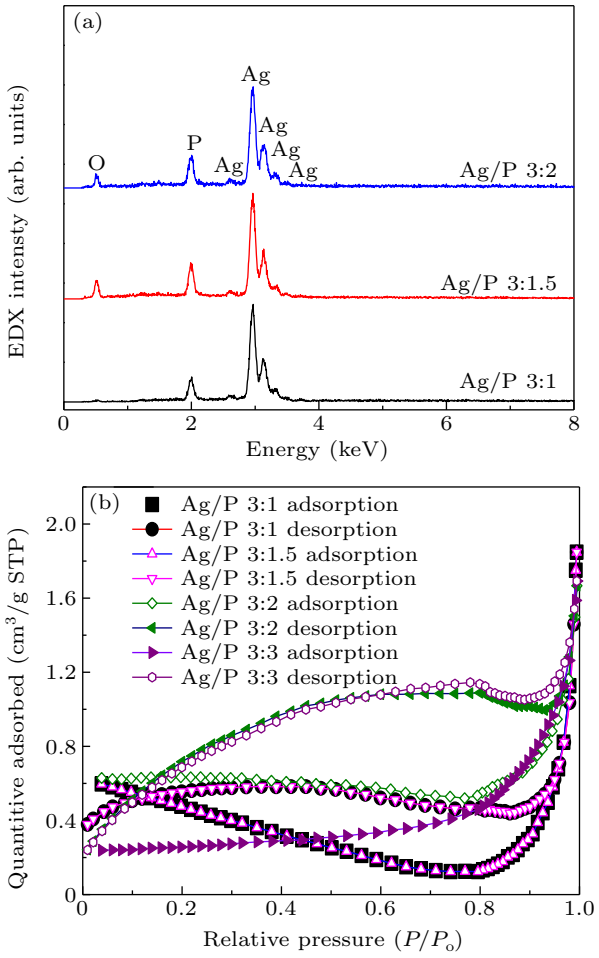


Fig. 3. (a) EDX analysis and (b) BET results of as-synthesized Ag_3PO_4 with different Ag^+/PO_4^{3-} ratios in precursor solution (Ag^+/PO_4^{3-} = 3:1; 3:1.5; 3:2; 3:3).

Raman spectroscopy of the fabricated samples was performed to help detect small changes in the crystal lattice and is shown in Fig. 5. In the wavenumber range of 100 cm^{-1}–1100 cm^{-1}, samples exhibited 5 Raman peaks at 223 cm^{-1}, 398 cm^{-1}, 551 cm^{-1}, 906 cm^{-1}, and 1064 cm^{-1}: most of them are low in intensity, except the peak at 906 cm^{-1}. The low peak at 223 cm^{-1} was assigned to the vibration mode (rotation or translation) of the tetrahedron [PO_4], while

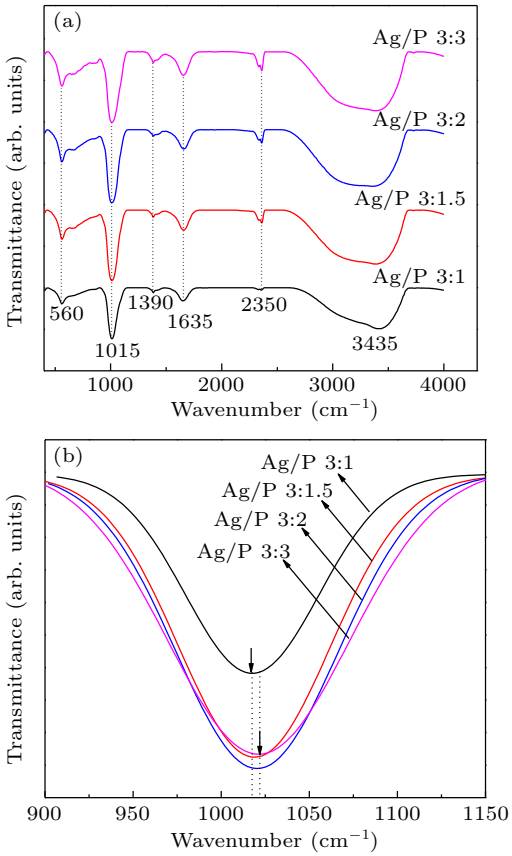


Fig. 4. (a) FTIR spectra of as-synthesized Ag_3PO_4 with different Ag^+/PO_4^{3-} ratios in precursor solution (Ag^+/PO_4^{3-} = 3:1; 3:1.5; 3:2; 3:3) and (b) a comparison of the 1015 cm^{-1} peak position.

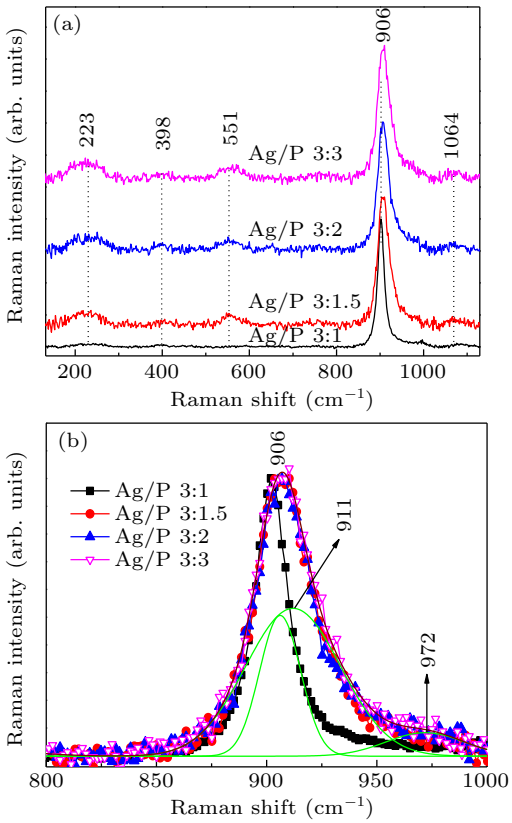


Fig. 5. (a) Raman scattering spectra of as-synthesized Ag_3PO_4 with different Ag^+/PO_4^{3-} ratios in precursor solution (Ag^+/PO_4^{3-} = 3:1; 3:1.5; 3:2; 3:3) and (b) a comparison of the 906 cm^{-1} vibration peak.

the 398 cm^{-1} and 551 cm^{-1} peaks were the symmetric (E) and asymmetric (T_2) bending modes of the [PO_4] cluster, respectively.[30] It is observed that the intense peak at 906 cm^{-1} not only shifts towards the high wave number (902 cm^{-1} for the Ag/P 3:1 sample and 906 cm^{-1} for the Ag/P 3:3 sample), but also expands and becomes asymmetric as the Ag^+/PO_4^{3-} ratio decreases. Figure 5(b) depicts in detail the peak at 906 cm^{-1}, which shows that the 906 peak consists of three components of 906 cm^{-1}, 911 cm^{-1}, and 972 cm^{-1}. They can be attributed to symmetric stretching vibration (A_1) and two asymmetric stretching modes (T_2) of the [PO_4] group,[30] respectively. The shift of the 906 cm^{-1} peak is in an agreement with the XRD and FTIR results, which both confirm the small deformation of the crystal lattice upon the Ag^+/PO_4^{3-} change in precursor solution.

Table 2. The area ratio of the Ag^o and Ag^+ XPS peaks (Ag^o:Ag^+) for the two spin orbit states Ag $3d_{1/2}$ and Ag $3d_{3/2}$ in the Ag/P 3:1 and Ag/P 3:1.5 samples.

Sample	Area ratio Ag^o:Ag^+ (%)	
	Ag $3d_{1/2}$	Ag $3d_{3/2}$
Ag/P 3:1	3.4%	3.1%
Ag/P 3:1.5	1.9%	1.2%

X-ray photoelectron spectroscopy (XPS) measurements with an energy resolution of 0.1 eV were performed to investigate the composition of chemical elements on the surfaces of the as-synthesized samples and to monitor the changes between their bonds (Fig. 6). The XPS spectra were calibrated with respect to the binding energy of the adventitious C 1s peak at 284.8 eV. Figure 6(a) shows the survey XPS spectra for the Ag/P 3:1 and Ag/P 3:1.5 samples, which indicate the existence of all the required elements in the photocatalyst, i.e., Ag, P, and O. The appearance of the C 1s peak at 284.8 eV is due to the inherent presence of absorbed CO_2 molecules on the surface of the material, or even originates from the adventitious hydrocarbon in the XPS instrument. The relevant high-resolution XPS spectra of the constituent elements Ag, O, and P are shown in Figs. 6(b)–6(d), respectively. The peaks at binding energies of 367.6 eV and 373.6 eV were assigned to the Ag $3d_{5/2}$ and Ag $3d_{3/2}$ states, which are characteristic of Ag^+ ions (Fig. 6(b)).[31] Based on the asymmetry of the XPS peak, very small peaks at 369.5 eV and 375.4 eV were found, which are believed to correspond to the metallization Ag^o state. The amount of metallization in the Ag/P 3:1 and Ag/P 3:1.5 samples was evaluated by calculating the area ratio of the Ag^o and Ag^+ peaks. Table 2 shows that the Ag^o/Ag^+ ratio is above 3% for the Ag/P 3:1 sample and falls below 2% for the Ag/P 3:1.5 sample. This suggests that the metallization of the Ag^+ ion decreases with increasing PO_4^{3-} concentration to the excess level, which is consistent with the aim of the study. Figure 6(c) depicts the XPS spectra of the O 1s state, which includes some constituent peaks. The O1 peak at 530.2 eV could

be assigned to O–Ag bonding, while the O2 peak at 532.2 eV is related to the dissociated OH group of H_2O adsorbed on the Ag_3PO_4 surface.[32] Figure 6(d) presents the high-resolution XPS spectrum of the P 2p state of the Ag/P 3:1 and Ag/P 3:1.5 samples. The spectrum includes 2 peaks at 132.5 eV and 134.0 eV for the P $2p_{3/2}$ state and P $2p_{1/2}$, respectively. These peaks shift towards the higher binding energies of 133.3 eV and 134.5 eV for the Ag/P 3:1.5 sample, which is likely due to the compression of the tetrahedron [PO_4], as shown in the XRD, FTIR and Raman results.

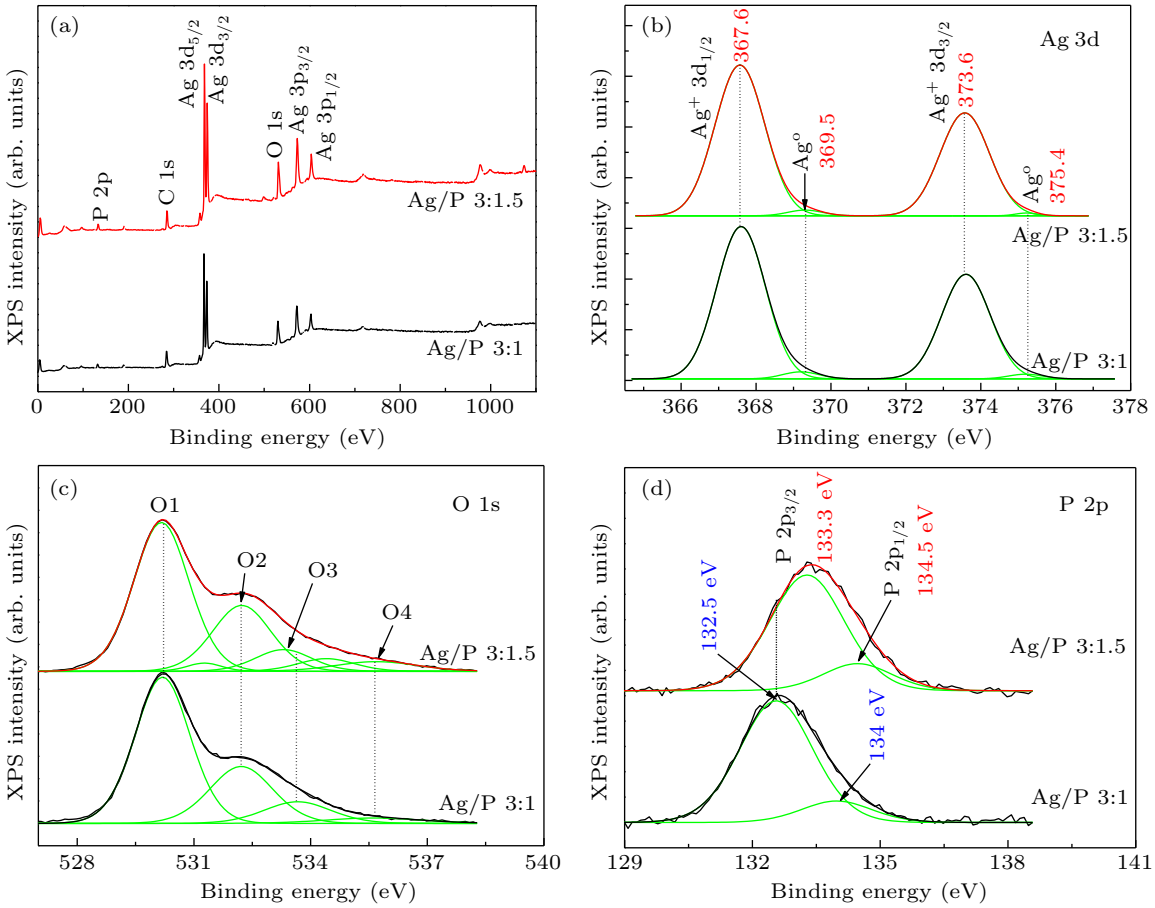


Fig. 6. (a) XPS survey spectra of as-synthesized Ag_3PO_4 with different Ag^+/PO_4^{3-} ratios in precursor solution (Ag^+/PO_4^{3-} = 3:1; 3:1.5; 3:2; 3:3), and the relevant high-resolution XPS spectra of the constituent elements of (b) Ag, (c) O, and (d) P.

UV-vis absorption spectroscopy was performed to determine the optical absorption and energy bandgap of as-synthesized APO, as shown in Fig. 7(a). All the samples exhibit strong absorption at a wavelength shorter than 520 nm, demonstrating that visible radiation can be effectively used in the photoexcitation. Using the Kubelka–Munk function, the band gap E_g can be determined from the plot of $(\alpha h\nu)^{1/2}$ as a function of the photon energy (hc/λ) for the indirect semiconductor, as shown in Fig. 7(b). The results show that the energy band gap is 2.43 eV, which is in a good agreement with previous reports.[31,33] As the PO_4^{3-} concentration increases, the absorbance for wavelengths less than 530 nm increases while the absorption background (above 530 nm) decreases. This is consistent with higher crystallinity as the PO_4^{3-} concentration increases, as observed above.

As photoluminescence (PL) results from recombination of excited electrons and holes, room-temperature photoluminescence spectra were measured (excitation wavelength of 350 nm) to help to evaluate the separation efficiency of photoexcited charge carriers in the as-synthesized APO samples, as shown in Fig. 8(a). The results show that all the APO samples fluoresce in a wide range from 400 nm to 700 nm, with a strong emission peak around 520 nm (corresponding to the band gap of 2.43 eV for APO material). It is observed that the Ag/P 3:1 and Ag/P 3:1.5 samples possessed the weakest PL intensity, suggesting the lowest electron/hole recombination rate, which is beneficial for the enhancement of photocatalytic activity. In addition, the normalized PL spectra in Fig. 8(b) show a shift of the PL emission peaks towards a larger wavelength as the ratio of the Ag^+/PO_4^{3-} decreased, which was most pronounced for the Ag/P 3:2 sample.

The photocatalytic performance of the APO samples under visible light irradiation was evaluated through the decomposition of 10 ppm RhB without any additional sacrificial reagents using xenon lamp illumination. Figure 9(a) shows curves representing the relative C/C_o ratios of RhB in solution

over time. Before light irradiation, the solutions were magnetically stirred in the dark for 30 min to achieve adsorption–desorption equilibrium. The results showed that the APO samples quickly reached the saturated adsorption state in less than 10 minutes, with an adsorption rate of about 10% of the RhB concentration in the solution. The low RhB adsorption rate of the samples could be explained by the very low specific surface area, as observed in the BET measurements. When illuminated, all the synthesized APO samples showed strong photocatalytic performance, completely decomposing RhB in less than 30 min, especially for the Ag/P 3:1.5 sample in only about 15 minutes. It is worth noting that the samples synthesized under PO_4^{3-} excess conditions showed greater photocatalytic efficiency than the samples with the Ag^+/PO_4^{3-} ratio of 3:1. This can be explained by the high crystallinity of APO, as observed in the XRD results, and the low rate of electron–hole recombination, as in the PL results. However, together with good crystallization, the samples fabricated in PO_4^{3-} excess solution also had a sharp increase in particle size, as indicated in the SEM results, which limited the photocatalytic efficiency due to the small specific surface area. As a result, the Ag/P 3:1.5 sample has the strongest photocatalytic activity because of both good crystallinity and small particle size.

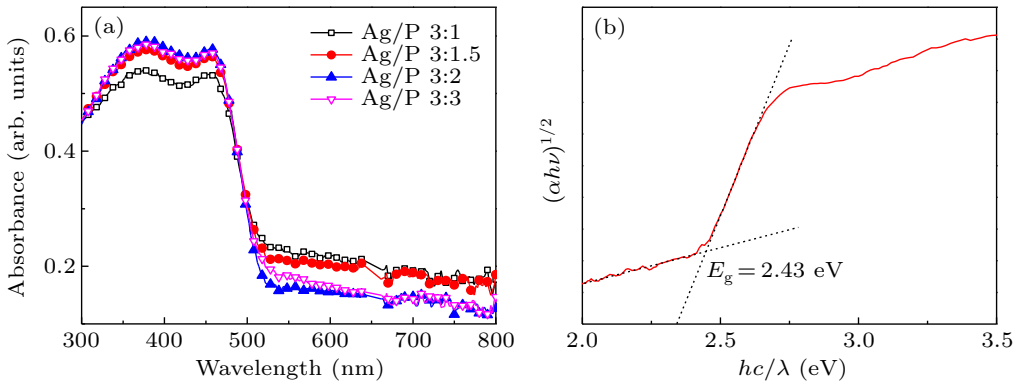


Fig. 7. (a) UV-vis absorption spectra of as-synthesized Ag_3PO_4 with different Ag^+/PO_4^{3-} ratios in precursor solution (Ag^+/PO_4^{3-} = 3:1; 3:1.5; 3:2; 3:3) and (b) the method to determine the energy band gap from the plot of $(\alpha h\nu)^{1/2}$ versus photon energy hc/λ.

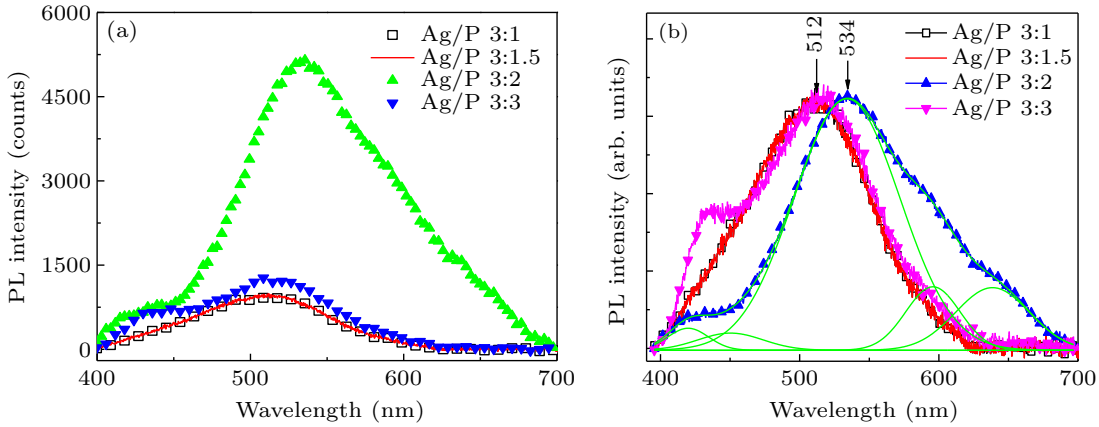


Fig. 8. (a) PL spectra of as-synthesized Ag_3PO_4 with different Ag^+/PO_4^{3-} ratios in precursor solution (Ag^+/PO_4^{3-} = 3:1; 3:1.5; 3:2; 3:3) and (b) the normalized PL spectra.

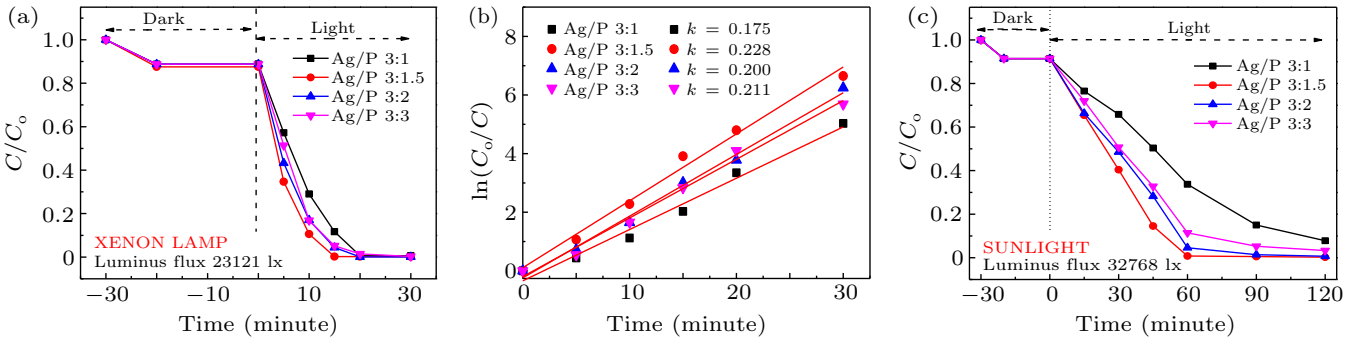


Fig. 9. (a) Photocatalytic activities and (b) reaction rates of as-synthesized Ag_3PO_4 in decomposing RhB solution under visible light using a xenon lamp; (c) photocatalytic activities under natural sunlight.

The pseudo-first-order kinetic model is used to determine the photocatalytic reaction rate, $\ln(C_o/C) = kt$, where the rate constant k can be achieved from the slope of the linear relationship of the plot $\ln(C_o/C) = kt$ versus reaction time (Fig. 9(b)). The catalysts exhibit the reaction rate constants $k \sim 0.228$, 0.211, 0.200, 0.175 for Ag/P 3:1.5, Ag/P 3:3, Ag/P 3:2, and Ag/P 3:1, respectively. To assess the practical applicability of the as-synthesized APO, the photocatalytic decomposition of RhB was performed under illumination of natural sunlight at noon (Fig. 9(c)). The samples exhibit excellent photocatalytic activity under sunlight. The sample with the highest photocatalytic efficiency is still Ag/P 3:1.5, which completely decomposes RhB dye in 60 minutes, and the sample with the lowest photocatalytic efficiency is still Ag/P 3:1, which decomposes over 90% RhB within 120 minutes. The order of samples with photocatalytic efficiency going from strong to weak is similar to that of the photocatalysis test under the xenon lamp.

4. Conclusion

The spherical nanoparticle Ag_3PO_4 was successfully synthesized using a facile co-precipitation method with Ag^+/PO_4^{3-} ratios of 3:1, 3:1.5, 3:2, and 3:3. The excess concentration of PO_4^{3-} in the precursor solution reduces the lattice constant, increases the crystallinity and particle size, and increases the photocatalytic activity of Ag_3PO_4 compared with that with the Ag^+/PO_4^{3-} ratio of 3:1. The Ag/P 3:1.5 sample exhibited the strongest photocatalytic activity due to its high crystallinity, small particle size and lowest electron–hole recombination rate. This study shows the practical applicability of Ag_3PO_4 material for photocatalytic degradation of polluted organic substances in the natural environment using sunlight.

Acknowledgment

Project supported by a scientific and technological project at the level of Ministry of Education and Training (Grant No. B2020-MDA-11).

References

[1] Yi Z, Ye J, Kikugawa N, Kako T, Ouyang S, Stuart-Williams H, Yang H, Cao J, Luo W, Li Z, Liu Y and Withers R L 2010 *Nat. Mater.* **9** 559
[2] Chen X, Dai Y and Wang X 2015 *J. Alloys Compd.* **649** 910
[3] Deng J, Pang H, Deng D and Zhang J 2012 *Proceedings of the Institution of Mechanical Engineers, Part N: Journal of Nanoengineering and Nanosystems* **225** 67
[4] Huang G F, Ma Z L, Huang W Q, Tian Y, Jiao C, Yang Z M, Wan Z and Pan A 2013 *J. Nanomater.* **2013** 371356
[5] Batvandi M, Haghighatzadeh A and Mazinani B 2020 *Appl. Phys. A* **126** 7
[6] Dong P, Hao Y, Gao P, Cui E and Zhang Q 2015 *J. Nanomater.* **2015** 857506
[7] Amornpitoksuk P, Intarasuwan K, Suwanboon S and Baltrusaitis J 2013 *Ind. Eng. Chem. Res.* **52** 17369
[8] Dong L, Wang P, Wang S, Lei P and Wang Y 2014 *Mater. Lett.* **134** 158
[9] Febiyanto F and Sulaeman U 2020 *Jurnal Kimia Valensi* **6** 1
[10] Afifah K, Andreas R and Hermawan D 2019 *Bull. Chem. React. Eng. Catal.* **14** 625
[11] Yang Z M, Liu Y Y, Xu L, Huang G F and Huang W Q 2014 *Mater. Lett.* **133** 139
[12] Guan X, Shi J and Guo L 2013 *Int. J. Hydrog. Energy* **38** 11870
[13] Futihah I, Riapanitra A, Yin S and Sulaeman U 2020 *J. Phys. Conf. Ser.* **1494** 012027
[14] Liu Q, Li N, Qiao Z, Li W, Wang L, Zhu S, Jing Z and Yan T 2019 *Front. Chem.* **7** 866
[15] Yan T, Guan W, Li W and You J 2014 *RSC Adv.* **4** 37095
[16] Qin J, Zhang X, Yang C, Song A, Zhang B, Rajendran S, Ma M and Liu R 2016 *Funct. Mater. Lett.* **09** 1650063
[17] Febiyanto F, Soleh A, Amal M S K, Afif M, Sewiji S, Riapanitra A and Sulaeman U 2019 *Bull. Chem. React. Eng. Catal.* **14** 1
[18] Liang Q, Shi Y, Ma W, Li Z and Yang X 2012 *Phys. Chem. Chem. Phys.* **14** 15657
[19] Liu M, Wang G, Xu P, Zhu Y and Li W 2020 *Appl. Sci.* **10** 9
[20] Zhang M, Du H, Ji J, Li F, Lin Y C, Qin C, Zhang Z and Shen Y 2021 *Molecules* **26** 7
[21] Osman N S, Sulaiman S N, Muhamad E N, Mukhair H, Tan S T and Abdullah A H 2021 *Catalysts* **11** 4
[22] Panthi G, Gyawali K R and Park M 2020 *Nanomaterials* **10** 5
[23] Xie Y P and Wang G S 2014 *J. Colloid Interface Sci.* **430** 1
[24] Shi L, Liang L, Ma J, Wang F and Sun J 2014 *Dalton Trans.* **43** 7236
[25] Tseng C S, Wu T and Lin Y W 2018 *Materials* **11** 5
[26] Zwara J, Grabowska E, Klimczuk T, Lisowski W and Zaleska-Medynska A 2018 *J. Photochem. Photobiol. A: Chem.* **367** 240
[27] Infrared Spectroscopy 2020
[28] Aufort J, Lebon M, Gallet X, Ségalen L, Gervais C, Brouder C and Balan E 2018 *American Mineralogist* **103** 326
[29] Destainville A, Champion E, Bernache-Assollant D and Laborde E 2003 *Mater. Chem. Phys.* **80** 269
[30] Trench A B, Machado T R, Gouveia A F, Assis M, da Trindade L G, Santos C, Perrin A, Perrin C, Oliva M, Andrés J and Longo E 2018 *Appl. Catal. B: Environmental* **238** 198
[31] Song L, Yang J and Zhang S 2017 *Chem. Eng. J.* **309** 222
[32] Chong R, Cheng X, Wang B, Li D, Chang Z and Zhang L 2016 *Int. J. Hydrog. Energy* **41** 2575
[33] Liu Y, Qian Q, Yi Z, Zhang L, Min F and Zhang M 2013 *Ceram. Int.* **39** 8513